Molecular Therapy
Nucleic Acids
Original Article

MicroRNA-206 Downregulation Improves Therapeutic Gene Expression and Motor Function in *mdx* Mice

Karen Bulaklak,[1] Bin Xiao,[1] Chunping Qiao,[1] Jianbin Li,[1] Tejash Patel,[1] Quan Jin,[1] Juan Li,[1] and Xiao Xiao[1]

[1]Division of Pharmacoengineering and Molecular Pharmaceutics, Department of Pharmaceutical Sciences, Eshelman School of Pharmacy, University of North Carolina at Chapel Hill, Chapel Hill, NC, USA

Duchenne muscular dystrophy (DMD) is a severe muscle-wasting disorder caused by a mutation in the dystrophin gene. Numerous gene therapies have been developed to replace or repair the defective dystrophin gene; however, these treatments cannot restore the full-length protein or completely resolve dystrophic symptoms. Secondary pathological mechanisms, such as functional ischemia and fibrosis, are thought to exacerbate the primary defect and cause the profound muscle degeneration found in dystrophic muscle. Surrogate therapies utilizing alternative therapeutic genes, or "booster genes," such as VEGFA and utrophin, seek to address these secondary mechanisms and have shown impressive benefit in *mdx* mice. A skeletal muscle-specific microRNA, miR-206, is particularly overexpressed in dystrophic muscle and inhibits the expression of known booster genes. Thus, we aimed to determine if miR-206 contributes to dystrophic pathology by repressing beneficial gene expression. Here, we show that AAV-mediated expression of a miR-206 decoy target effectively downregulated miR-206 expression and increased endogenous therapeutic gene expression in mature *mdx* muscle. Furthermore, treatment significantly improved motor function and dystrophic pathology in *mdx* mice. In summary, we have identified a contributing factor to the dystrophic phenotype and characterized a novel therapeutic avenue for DMD.

INTRODUCTION

Duchenne muscular dystrophy (DMD) is a severe muscle-wasting disease affecting approximately 1 in 5,000 male live births. It is caused by a mutation in the gene encoding dystrophin, which forms an essential linkage between the outer extracellular matrix and cytoskeletal actin filaments. The loss of dystrophin renders the muscle fiber highly susceptible to contraction-induced damage. As a result, DMD patients progressively lose muscle mass and become non-ambulatory in their early teens. Even with supportive therapies, patients die prematurely in their 30s or 40s due to respiratory or cardiac complications.[1] The severity of this disease and lack of effective therapies that target the underlying cause warrant investigation into better treatment strategies.

Gene therapies aimed at replacing or correcting the defective dystrophin gene have shown promise for DMD. Recombinant adeno-associated viruses (rAAVs) are popular gene-delivery vehicles due to their non-pathogenic nature and ability to efficiently transduce and persist in muscle.[2] AAV-mediated expression of truncated dystrophin proteins and delivery of exon-skipping constructs have shown significant benefits in animal models of DMD.[3–7] Still, dystrophin-targeted therapies come with many challenges and cannot completely ameliorate symptoms. For example, expression of truncated dystrophin fails to prevent joint contractures and cardiomyopathy in Golden Retriever muscular dystrophy (GRMD) dogs.[8] Furthermore, current gene therapy strategies do not restore the full-length protein (427 kDa) and aim to create a milder phenotype similar to Becker muscular dystrophy (BMD). Immune reactions to the recombinant dystrophin protein have also been reported in clinical trials.[9] This has spurred further exploration into alternative therapies that can address these shortcomings.

Several studies have shown that the profound muscle degeneration observed in DMD results from secondary pathological mechanisms that exacerbate the primary genetic defect, such as reduced blood flow (functional ischemia), inflammation, and fibrosis.[10–14] Surrogate therapies that involve the use of "booster genes," or genes aside from dystrophin to target secondary disease mechanisms, can effectively alleviate dystrophic symptoms.[15] For example, overexpression of vascular endothelial growth factor A (VEGFA) increases capillary density to improve blood flow to the muscle, which reduced muscle necrosis and increased regeneration in *mdx* mice.[16] Multiple groups have also found methods to increase levels of dystrophin paralog utrophin, which is normally expressed at the neuromuscular junction (NMJ). Sarcolemmal expression of utrophin has been shown to increase membrane integrity, improving strength and inhibiting progression of dystrophic symptoms in DMD models.[17–21] All together, surrogate therapies can effectively alleviate symptoms and are useful alternatives to dystrophin replacement.

Received 8 January 2018; accepted 14 May 2018;
https://doi.org/10.1016/j.omtn.2018.05.011.

Correspondence: Xiao Xiao, Division of Pharmacoengineering and Molecular Pharmaceutics, Department of Pharmaceutical Sciences, Eshelman School of Pharmacy, University of North Carolina at Chapel Hill, 2077 Genetic Medicine Building, 120 Mason Farm Road, Chapel Hill, NC 27599 USA.
E-mail: xxiao@email.unc.edu

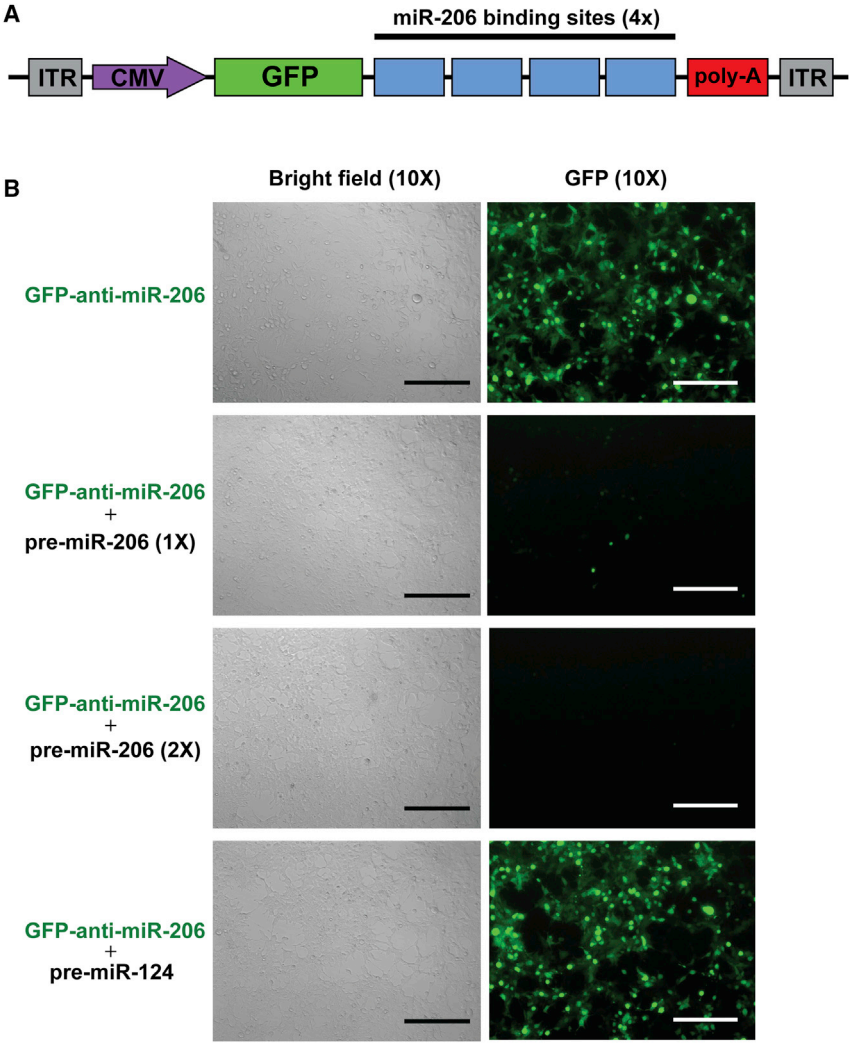

Figure 1. Vector Construct Design and Specificity

(A) AAV-anti-miR-206 vector construct design. Four tandem repeats of the antisense sequence against miR-206 were cloned into a vector plasmid containing a CMV promoter, GFP expression marker (truncated sequence not shown), and ending with a poly(A) signal. (B) Anti-miR-206 specificity was tested by co-infection in HEK293 cells. Cells were transduced with AAV2-GFP-anti-miR-206 alone (MOI, 10^6 vg/cell, first row) or in combination with AAV2-pre-miR-206 (MOI, 10^6 vg/cell, second row; and MOI, 2×10^6 vg/cell, third row) or AAV2-pre-miR-124 (MOI, 10^6 vg/cell, last row). Co-transduction with miR-206 precursor diminished GFP expression, while miR-124 did not affect GFP signal. Magnification, 10×; scale bars, 300 μm.

MicroRNAs (miRs) are short (~22 nt), non-coding RNA molecules that are important regulators of gene expression. Their main function is to inhibit gene expression through binding of the RNA-induced silencing complex (RISC), which subsequently interferes with the stability and proper translation of target mRNAs that harbor complementary sequences in their 3′ UTR.[22] A shared miR profile has been identified in both *mdx* mice and DMD patients.[23] A skeletal muscle-specific miR, miR-206, is particularly elevated in dystrophic muscle.[24] Under normal conditions, miR-206 is highly expressed in muscle precursor satellite cells and works to inhibit Pax7 expression to drive differentiation.[25] However, previous work has shown that miR-206 inhibits therapeutic booster genes, including VEGFA and utrophin.[25–27] Thus, we hypothesized that downregulation of miR-206 in *mdx* muscle via AAV-mediated expression of a decoy target would allow therapeutic gene expression and improve muscle function. We also aimed to elucidate the role of miR-206 in dystrophic pathology and secondary disease mechanisms, including impaired muscle vascularization and increased muscle fibrosis. Findings from this study would aid in better understanding of a previously unexplored aspect of pathology and characterize a novel therapeutic paradigm for DMD.

RESULTS

AAV-Anti-miR-206 Inhibits miR-206 Expression

A vector plasmid, "anti-miR-206," was generated to express a decoy target mRNA to competitively bind excess miR-206. Four tandem repeats of the exact miR-206 seed sequence were placed in the 3′ UTR of a GFP reporter gene. The construct was subsequently packaged into the AAV2 capsid for *in vitro* analyses (Figure 1A). To determine whether this construct bound exclusively to miR-206, a series of co-transductions were performed in HEK293 cells. Administration of AAV2-GFP-anti-miR-206 alone induced high reporter gene expression at 48 hr (Figure 1B, top row). Co-administration with an AAV2 harboring a precursor (pre) miR-206 sequence inhibited GFP expression (Figure 1B, second row), and higher levels of pre-miR-206 virus completely eliminated vector plasmid expression (Figure 1B, third row). In contrast, the addition of non-specific pre-miR-124 had no effect on GFP expression (Figure 1B, bottom row).

AAV9-Anti-miR-206 Treatment Improves Motor Deficits in *mdx* Mice

At 8 weeks of age, *mdx* mice were treated with PBS, an AAV9 vector containing a truncated GFP reporter gene sequence ("Sham vector"), or an AAV9 vector harboring a truncated GFP reporter gene with miR-206 binding regions in its 3′ UTR ("anti-miR-206") at a dose of 1×10^{12} vector genomes (vg) per mouse. Motor function was evaluated biweekly by rotarod testing to determine balance, grip force, and motor coordination as well as grip force testing to determine forelimb strength. Compared to PBS- and sham vector-treated mice, anti-miR-206 treatment significantly improved *mdx* rotarod running time at 1 month (**p = 0.0105; Figure 2A) and 5 months post-treatment (**p = 0.0044 and **p = 0.0038, versus PBS and sham vector,

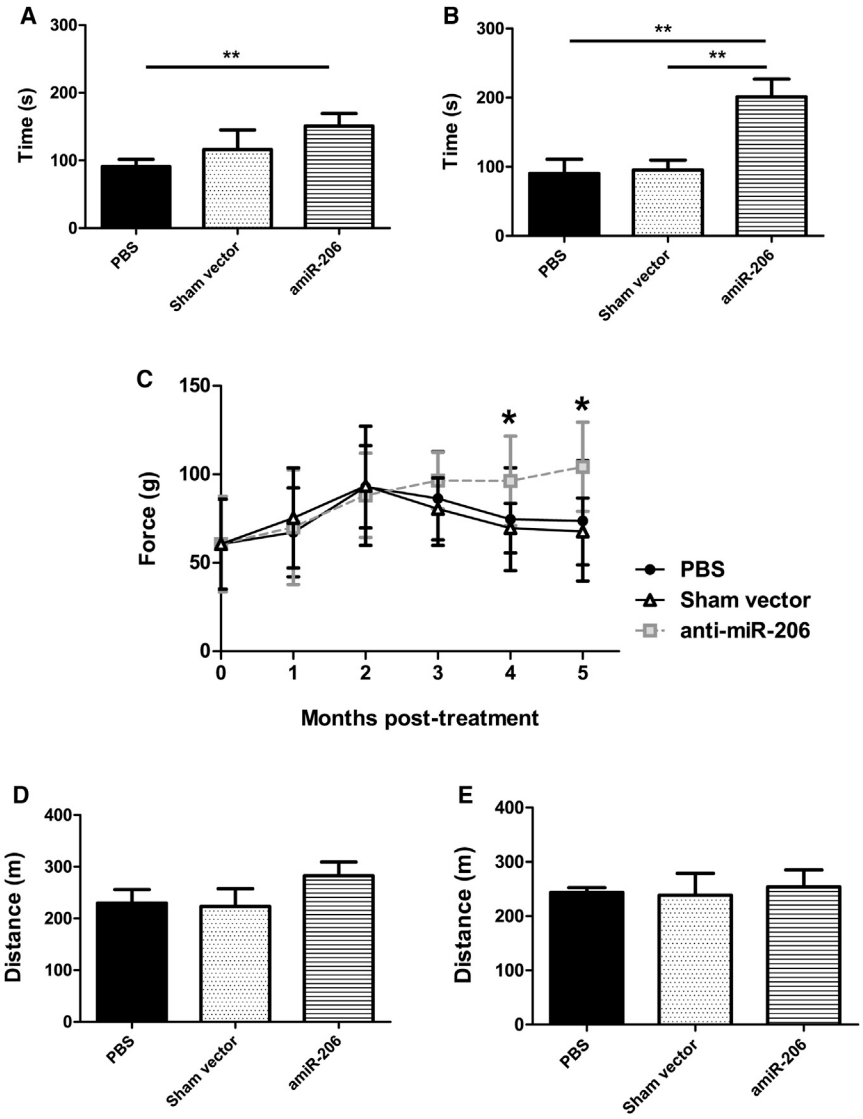

Figure 2. Effect of miR-206 Reduction on Motor Function

(A) Rotarod running time of *mdx* at 1 month post-treatment. Mice were treated with PBS ("untreated"), AAV9 sham vector, or AAV9-anti-miR-206. A significant improvement in running time was observed with AAV9-anti-miR-206 treatment compared to the PBS control (**p = 0.0105, n = 6 for all groups). (B) Rotarod running time of *mdx* at 5 months post-treatment. Anti-miR-206 treatment significantly increased run time compared to control groups (anti-miR-206 versus PBS, **p = 0.0044, n = 6 for both groups; anti-miR-206 versus vector control, **p = 0.0038, n = 6 for both groups). (C) Absolute grip force over time. A significant improvement in forelimb strength was observed at 4 and 5 months post-treatment (*p < 0.05, n = 6 for all groups). (D) Treadmill run distance at 1 month post-treatment. No significant differences were found between groups (p > 0.05, n = 6 per group). (E) Treadmill run distance at 5 months post-treatment. No obvious differences were seen with or without treatment (p > 0.05, n = 6 per group). Each bar represents mean (+SEM).

respectively; Figure 2B). Rotarod performance did not change with PBS or sham vector treatment. Significant improvements in forelimb strength with anti-miR-206 treatment were also observed at 4 and 5 months post-treatment (*p < 0.05; Figure 2C). At the same time, strength steadily declined in the PBS and sham vector groups. There were no significant changes in treadmill performance between any *mdx* groups at either 1 (Figure 2D) or 5 months (Figure 2E) post-treatment.

AAV9-Anti-miR-206 Knocks Down miR-206 Expression in *mdx* Muscle and Increases Target Gene Expression

Diaphragm muscle was extracted from age-matched wild-type (C57BL/6, "WT"), PBS ("untreated"), and treated *mdx* mice at 3 months after vector administration to measure miR-206 levels. Since the sham vector had no effect on motor function compared to PBS alone, only PBS-treated mice were used as a control for further studies.

Relative qPCR revealed that WT muscle contained low levels of miR-206 compared to *mdx* muscle, which was ~10 times greater at 3 months post-treatment (***p < 0.0001; Figure 3A). Administration of AAV9-anti-miR-206 decreased miR-206 content in *mdx* diaphragm by ~40% (*p = 0.0341) but did not reach WT levels. To determine the effect of miR-206 on therapeutic gene expression, two representative targets, Vegfa and utrophin (Utrn), were investigated for their demonstrated benefit for dystrophic pathology. Vegfa transcript levels were ~28% lower in *mdx* mice compared to WT (*p = 0.0157). AAV9-anti-miR-206 administration increased Vegfa transcription levels by ~61% over the untreated control (**p = 0.0026; Figure 3B). Utrophin mRNA in dystrophic mice were ~2-fold greater than in WT (***p < 0.0001) and almost doubled in response to miR-206 reduction (**p = 0.0012; Figure 3C). A significant increase in Utrn transcripts was also observed between WT and anti-miR-206-treated mice (***p < 0.0001).

miR-206 Knockdown Increases VEGF-A Expression and Induces Angiogenic Activity in Muscle

Western blotting was performed with tibialis anterior (TA) muscle lysates to measure VEGF-A expression in response to miR-206 regulation. Treatment increased VEGF-A protein in *mdx* muscle compared to either WT or untreated *mdx* samples (Figure 4A). To determine if treatment stimulated an angiogenic effect, immunofluorescent staining was performed to quantify capillaries in diaphragm muscle (Figure 4B). To determine capillary-to-fiber ratio, the fiber periphery was identified by green laminin staining, while

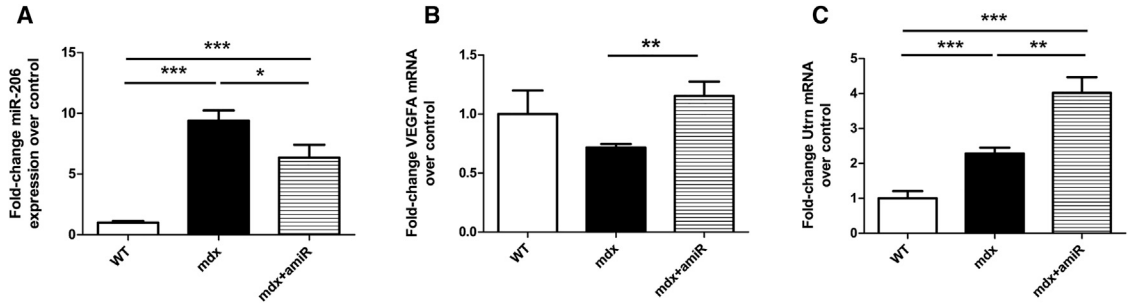

Figure 3. Effect of AAV-Anti-miR-206 Treatment on miR-206 and Target Transcript Levels *In Vivo*

(A) Wild-type (WT) DIA contained negligible amounts of miR-206, while significantly higher levels were found in untreated and treated *mdx* (***p < 0.0001, n = 6 per group). AAV9-anti-miR-206 treatment decreased miR-206 levels (*p = 0.00341, n = 6 per group). (B) AAV9-anti-miR-206 treatment significantly increased Vegfa mRNA in *mdx* mice compared to untreated *mdx* (**p = 0.0026, n = 6 per group). (C) Utrn transcript levels were elevated in treated *mdx* compared to both WT and untreated *mdx* groups (***p < 0.0001 and **p = 0.0012, respectively, n = 6 per group). Transcript levels were significantly higher in untreated *mdx* versus WT (***p < 0.0001, n = 6 per group). Each bar represents mean (±SEM).

capillaries were stained bright red (Figure 4C). Areas of diffuse, non-specific lectin staining were excluded from our calculations. The number of capillaries per fiber was reduced in dystrophic muscle compared to WT at 3 and 5 months post-treatment (***p = 0.0008 and **p = 0.0043, respectively; Figures 4D and 4E). Downregulation of miR-206 increased the ratio of vessels to fibers over the untreated group by ~30% and ~34% at 3 and 5 months post-treatment (***p < 0.0001 and *p = 0.0258, respectively). A modified Miles assay was performed to examine vessel integrity by measuring the amount of Evans blue (EB) dye leakage from the vessels into the surrounding muscle. Dye extravasation was examined in the quadricep (QUAD), hamstring (HAM), gastrocnemius (GAS), and TA. WT muscles contained low levels of infiltrating dye compared to *mdx* muscle groups at 3 and 5 months post-treatment (**p = 0.0094 and *p = 0.02220, respectively; Figures 4F and 4G). Vector administration significantly reduced dye penetration in all muscle groups compared to the untreated group, similar to that observed in WT muscle at both time points (*p = 0.0278 and *p = 0.0351 for 3 and 5 months, respectively).

Downregulation of miR-206 Enhances Utrophin Expression and Improves Muscle Pathology

Western blot using GAS muscle lysates at 3 months post-treatment demonstrated utrophin upregulation after anti-miR-206-treated mice compared to the untreated group (Figures 5A and 5B). Utrophin IF staining revealed a punctate staining pattern characteristic of the NMJ in WT and untreated *mdx* muscle (Figure 5C). In contrast, muscle treated with anti-miR-206 exhibited stronger NMJ staining and sarcolemmal localization of utrophin. H&E staining showed severe pathology in the dystrophic diaphragm consisting of actively degenerating (dark pink irregularly shaped and hypercontracted fibers) and regenerating fibers (smaller fibers with centrally located nuclei) and immune cell infiltration (groups of punctate blue staining in the endomysium) (Figure 5D, top row). Treatment appeared to reduce the severity of these symptoms. Compared to the diaphragm, GAS muscle pathology was milder in untreated *mdx* (Figure 5D, bottom row). Still, an improvement in muscle fiber morphology and organization was observed with anti-miR-206 treatment.

Decreased miR-206 Reduces Muscle Fibrosis in the Diaphragm and Hindlimb

To evaluate fibrosis in muscle, histological collagen staining was performed (Figure 6A). Both Masson trichrome and Picrosirius red and Fast green staining illustrated significant collagen deposition throughout the *mdx* diaphragm. In contrast, WT muscle contained little to no collagen staining. Collagen was still present with anti-miR-206 treatment, yet to a lesser degree. Collagen fibers stained with Picrosirius red appeared to be more diffuse in treated muscle compared to the untreated sample. Fibrotic area determined by quantifying Picrosirius red staining in the diaphragm and HAM muscles (Figures 6B and 6C, respectively). Little to no collagen staining was observed in the WT diaphragm but was present in ~10% of the HAM. Fibrosis occupied a significant area at ~35% of the *mdx* diaphragm and ~25% of the *mdx* HAM (***p < 0.0001 for both). With treatment, fibrotic area was significantly reduced in both the diaphragm and HAM (**p = 0.0043 and *p = 0.0279, respectively). Still, treated muscle contained significantly greater amounts of fibrosis compared to WT (***p < 0.0001 for the diaphragm and **p = 0.0046 for the HAM). Fibrosis was also measured in the diaphragm by quantifying hydroxyproline content, which is a major component of collagen. Consistent with the previous results, WT muscle contained low levels of hydroxyproline, while hydroxyproline was upregulated in dystrophic muscle (Figure 6D). However, a much larger increase was observed after 2 months in the untreated *mdx* muscle compared to treated muscle. Overall, miR-206 reduction appeared to hinder the development of fibrosis with time.

DISCUSSION

Secondary disease mechanisms promote DMD pathology by exacerbating muscle damage initiated by the primary dystrophin defect. Surrogate therapies that remediate these alternative pathways have greatly improved dystrophic symptoms. In the current study, we

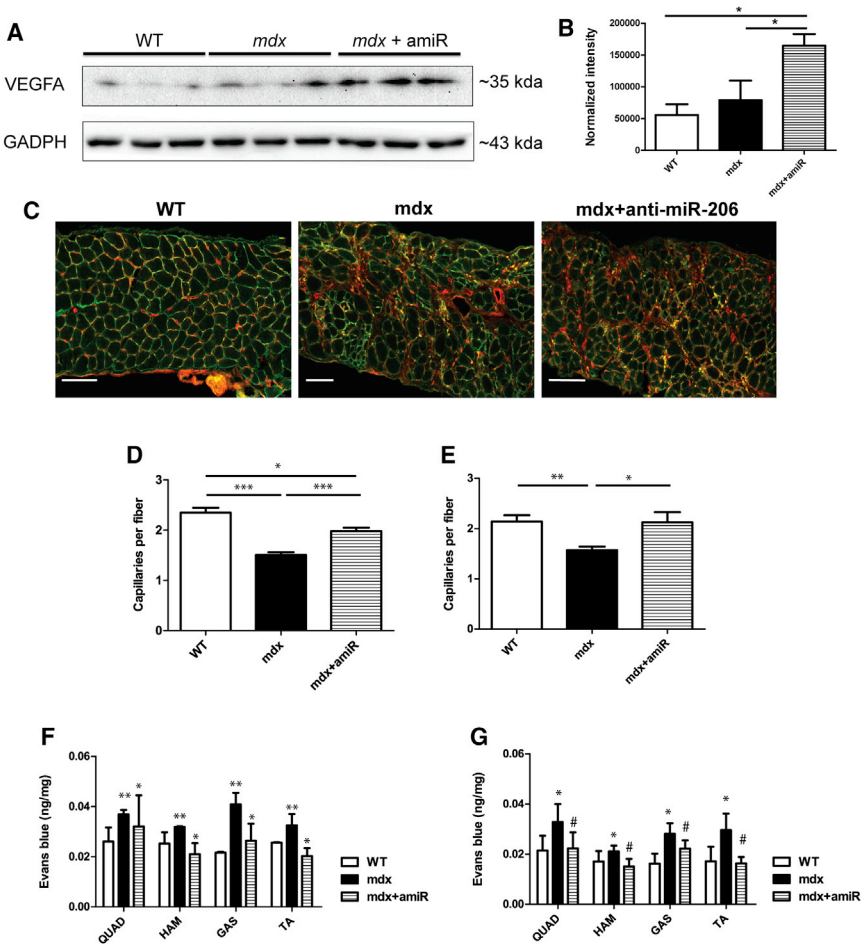

Figure 4. Effect of miR-206 Knockdown on VEGF-A Expression and Angiogenesis in Muscle

(A) Western blot results depicting VEGF-A expression in WT, untreated, and treated *mdx* muscle samples. VEGF-A expression was increased in treated *mdx* muscle versus WT or untreated *mdx*. (B) Densitometric analysis of VEGF-A western blot. A significant increase in VEGF-A expression was observed in treated *mdx* muscle compared to WT and untreated *mdx* (WT versus treated *mdx*, *p = 0.0218, and *mdx* versus treated *mdx*, *p = 0.0484, n = 3 for all groups). (C) Immunofluorescent staining images of diaphragm muscle lamina (green) and capillaries (punctate bright red staining) used for vessel density analysis. Magnification, 10×, scale bars, 100 μm. (D) Capillary-to-muscle fiber ratio at 3 months post-treatment. Vessel density was lower in untreated dystrophic muscle compared to WT (***p = 0.0008, n = 6 per group). A significant increase in vessels per fiber was observed in *mdx* mice with anti-miR-206 treatment versus the untreated group (***p < 0.0001, n = 6 per group). WT vessel density was slightly greater than treated *mdx* (*p = 0.0244, n = 6 per group). (E) Capillary-to-muscle fiber ratio at 5 months post-treatment. Again, treatment resulted in greater capillary density over the untreated *mdx* group (*p = 0.0258, n = 6 per group). WT muscle had significantly higher vessel density versus untreated *mdx* (**p = 0.0043, n = 6 per group). (F) A modified Miles assay was performed at 3 months post-treatment to measure vessel integrity across different muscle groups. Evans blue dye permeation was markedly greater in *mdx* muscle versus WT and anti-miR-206-treated muscle (**p = 0.0094 and *p = 0.0278, respectively, n = 6 for all groups). (G) Vessel integrity was again examined at 5 months post-treatment. Again, Evans blue dye content was greater in *mdx* muscle versus WT and anti-miR-206 treated muscle (*p = 0.0220 and #p = 0.0351, respectively, n = 6 for all groups). Each bar represents mean (±SEM).

explored the role of miR-206, which is upregulated in dystrophic muscle. Previous studies have attributed increased miR-206 levels to actively regenerating fibers; however, the role of miR-206 has not been adequately explored in the context of disease. In addition, several miR-206 targets have been used as booster genes to treat DMD, which prompted further investigation into its contribution to DMD pathology. Here, we sought to examine the involvement of miR-206 in secondary disease pathways as well as characterize a strategy for regulating its expression.

Manipulation of miR expression *in vivo* has been achieved through the use of "miR sponges," which act as decoy targets to derepress therapeutic gene expression.[28,29] Viral vectors have been employed to induce stable expression of these miR sponges for therapeutic applications, such as hepatocellular carcinoma and Alzheimer's disease.[30,31] Similarly, we show that miR-206 levels can be specifically decreased through AAV-mediated expression of a decoy target containing miR-206 binding sites in its 3′ UTR, which we termed "anti-miR-206." Administration of AAV9-anti-miR-206 to *mdx* mice significantly reduced miR-206 levels in the diaphragm, where miR-206 is known to be particularly elevated.[24] Through this method, miR-206 was not completely eliminated from the muscle. It is important to reiterate that recombinant AAVs can transduce mature muscle, yet gene transfer to regenerating muscle is inefficient.[32] Treated *mdx* muscle still contained significantly higher levels of miR-206 compared to WT, and regenerating fibers were abundant. Thus, our findings do not contradict those of Liu et al.,[33] which stress the importance of miR-206 in precursor cells for adequate muscle regeneration in DMD. A previous report by Anderson et al.[34] in *mdx* indicated that the level of muscle precursor proliferation does not differ drastically between the diaphragm and other muscles, which brings into question the contribution of muscle progenitors versus mature muscle to the observed quantities of miR-206. By using our AAV9-anti-miR-206 vector, we demonstrate that mature muscle also contributes to elevated miR-206 levels in dystrophic muscle.

Decreasing miR-206 in mature muscle improved motor deficits in *mdx* and prevented functional decline, which supports a therapeutic role for AAV9-anti-miR-206. The mild dystrophic phenotype of the *mdx*

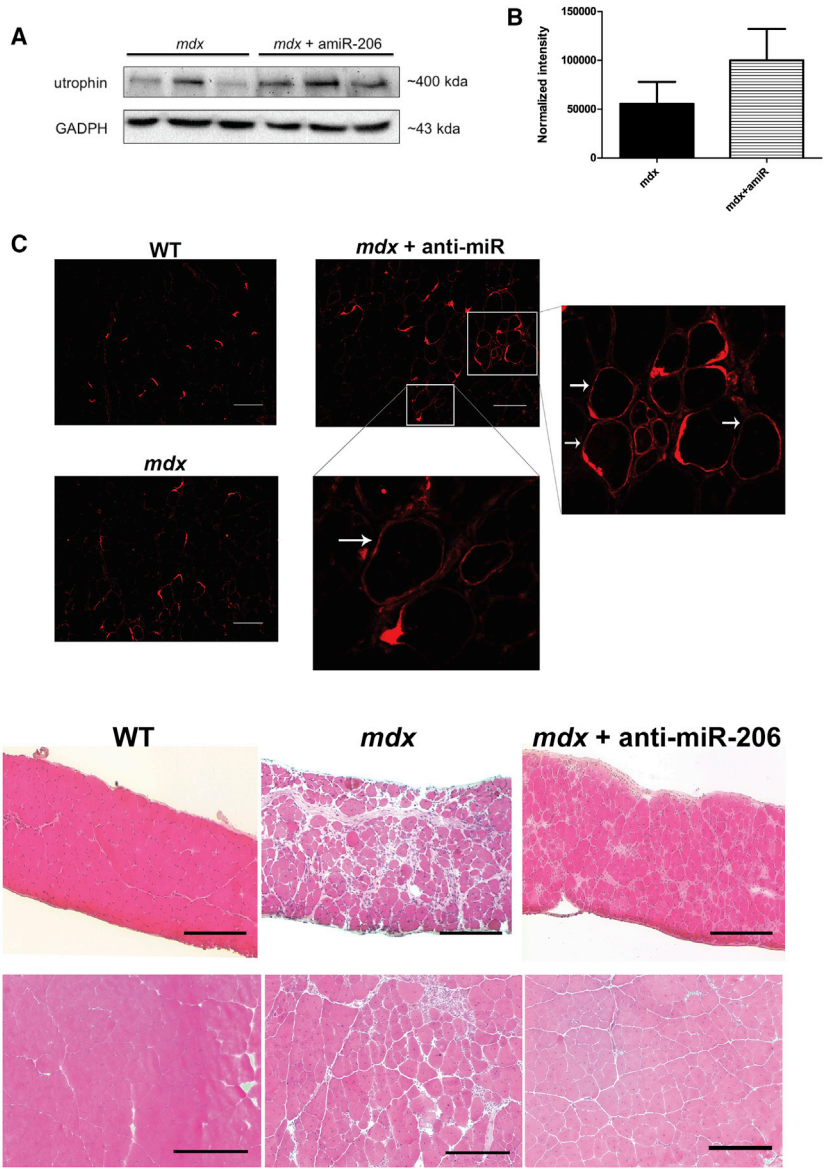

Figure 5. Effect of Decreased miR-206 on Utrophin Expression and Muscle Pathology

(A) Western blot detecting utrophin expression in untreated and treated *mdx* muscle. Utrophin levels were noticeably higher with treatment. (B) Densitometric analysis of utrophin western blot. A noticeable increase in utrophin expression was observed in treated *mdx* muscle compared to untreated *mdx* ($p = 0.3397$). Each bar represents mean (+SEM). (C) Utrophin immunostaining in muscle. Sarcolemmal staining was observed with treatment (white arrows). Utrophin staining was also stronger after treatment compared to WT and untreated *mdx* muscle. (D) H&E staining of WT, *mdx*, and treated *mdx* diaphragm (top row) and hamstring (bottom row) at 3 months post-treatment. Dystrophic muscle was characterized by necrotic and actively regenerating fibers and immune cell infiltration. Pathology was more severe in the diaphragm than the hindlimb. Treatment appeared to alleviate symptoms. Scale bars, 300 μm; magnification, 10×.

mouse was likely a factor in the absence of any noticeable differences in forelimb grip strength at earlier time points. Therapeutic benefits became more apparent with increasing age and strenuous exercise, suggesting that the treatment worked to prevent loss in strength caused by progressive pathology. Treadmill testing was performed to evaluate endurance as well as exacerbate muscle damage for better comparison of the untreated and treated groups. No differences were found in treadmill running with treatment, which can be explained by the lack of respiratory and cardiac deficiencies in these mice until later in life.[35] Interestingly, we saw no changes in rotarod performance in the control groups, but significant improvements with treatment over time. Since the rotarod also evaluates coordination and balance, these results may reflect better muscle function rather than strength.[36] To better understand the cause of these functional improvements, we explored the expression of two miR-206 targets, VEGFA and utrophin, and related therapeutic mechanisms.

In addition to downregulating miR-206 in the muscle, administration of AAV9-anti-miR-206 to *mdx* mice significantly increased transcript as well as protein levels of VEGF-A. In a study where VEGFA was overexpressed via rAAV, its angiogenic activity was utilized to increase vascularization in dystrophic muscle.[16] Similarly, we observed significant increases in capillary density with our treatment. Vessels formed under hypoxic disease conditions and in the presence of excess VEGF-A may be malformed and leaky.[37] After conducting Miles assays, we observed increased dye extravasation into the *mdx* muscle compared to the WT, which was decreased with treatment. While muscle vascularization and integrity were improved, there are remaining questions regarding treatment effect on muscle blood flow and why no changes were found in endurance. Previous reports have shown that *mdx* mice and DMD patients do not exhibit any differences in basal blood flow compared to normal controls, yet display significant differences in exercise-induced hyperemia.[10,38] The absence of membrane-associated neuronal nitric oxide synthase (nNOS) in dystrophic muscle prevents normal hemodynamic responses to exercise. Since our treatment does not address nNOS, it is understandable that blood flow regulation required for vigorous exercise would not be altered to induce any changes in treadmill performance. Pharmacological vasodilators have been utilized to address this, but improvements are transient and no long-term effects on pathology have been proven.[38,39] By increasing vessel density and integrity, we hoped to relieve functional ischemia, or the lack of

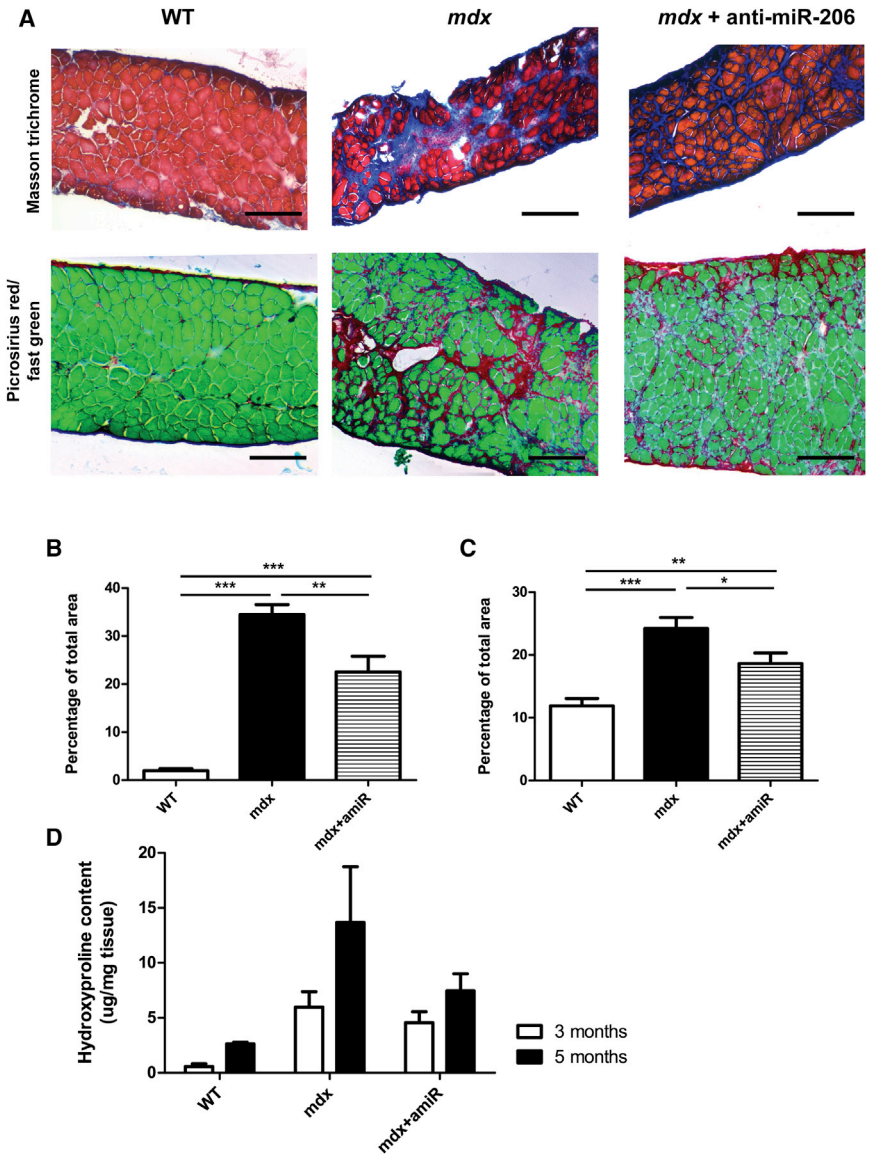

Figure 6. Effect of miR-206 Downregulation on Muscle Fibrosis

(A) Representative images of collagen staining in the diaphragm. Masson trichrome (top row) depicting collagen (blue) in the diaphragm muscle (red). Picrosirius red and Fast green staining (bottom row) showing collagen fibers (red) in the diaphragm muscle (green). Untreated *mdx* muscle displays considerable collagen accumulation compared to WT. Treatment appears to decrease fibrosis in muscle. Scale bars, 300 μm; magnification, 10×. (B) Picrosirius red quantitation in the diaphragm. The percentage of collagen staining was significantly higher in untreated and treated *mdx* muscle versus WT (***$p < 0.0001$ for both, $n = 6$). Compared to the untreated group, fibrotic area in treated *mdx* muscle was significantly decreased (**$p = 0.0043$, $n = 6$). (C) Picrosirius red quantitation in the hamstring. Collagen content in *mdx* muscle is again greater than WT (***$p < 0.0001$, $n = 6$). Treated muscle contained significantly less collagen than the untreated (*$p = 0.0279$, $n = 6$). There is a significant difference between WT and treated mice as well (**$p = 0.0046$, $n = 6$). (D) Hydroxyproline content was measured in WT, *mdx*, and treated *mdx* muscle at 3 and 5 months post-treatment. Hydroxyproline levels were much greater in dystrophic muscle, which increased over time. A considerable increase was observed in *mdx* muscle at 5 months, which was not as prominent with treatment. Each bar represents mean (±SEM).

proper blood flow to meet the metabolic demands of dystrophic muscle. Although no changes to muscle perfusion were reported with VEGF-A overexpression, Verma et al.[40] demonstrated in transgenic mdx/Flt-1 knockout mice that increasing capillary density can improve pathology, perfusion, and muscle contractile function. Despite differences in testing methodology, we found that our treatment was also beneficial for muscle pathology and motor function, which may be attributed in part to improvements in muscle vascularization.

Transgenic *mdx* models in which utrophin is upregulated as well as AAV-mediated microutrophin delivery have confirmed that utrophin overexpression can improve dystrophic symptoms.[18,19,21] Reduction of miR-206 in *mdx* muscle induced considerable increases in utrophin expression at the transcript and protein level compared to untreated *mdx*, with expression localized along the sarcolemma and heightened at the NMJ. Accordingly, overall muscle damage and subsequent fibrotic deposition were remediated, which would also work to improve functional deficits in the *mdx* mouse. Although sarcolemmal utrophin was not as widespread as with direct gene replacement, an ~2-fold increase over dystrophic levels can provide therapeutic benefit.[41] It is also possible that other derepressed miR-206 targets, such as VEGFA, could work in tandem to produce the improvements observed in this study. Utrophin increases at the NMJ also do not rule out the possibility of improved neuromuscular transmission with treatment, which may explain the enhanced balance and coordination of treated mice. In a similar fashion, expression of PGC-1α at the NMJ enhanced motor neuron activity and improved *mdx* muscle pathology and function.[42] The degree of miR-206 reduction with our treatment is likely not sufficient to induce utrophin levels needed for complete sarcolemmal distribution, and the drastic increases in transcript levels are not reflected in the amount of protein contained in the muscle, which indicates that translation is inhibited by an additional unknown mechanism. Still, our findings suggest that NMJ-associated utrophin expression could be suppressed in DMD. Utrophin expression in the muscle is nonetheless affected by the presence of miR-206, supporting its detrimental role in DMD.

Additional studies are needed for eventual translation of AAV9-anti-miR-206 treatment into the clinic. This would include exact miR-206 and target quantification, as well as verification of human miR-206 binding to the anti-miR-206 construct. Also, we chose to focus on two representative targets based on well-described therapeutic avenues for DMD; however, we cannot rule out the contribution of other miR-206 targets. We acknowledge that the improvements shown here may be indirectly related to the targets mentioned and further exploration into other affected miR-206 targets is thus warranted. The full potential of this treatment may also be obscured by insufficient depletion of miR-206. This is could be attributed partly to vector loss over time, which was more pronounced in the diaphragm than in the hindlimb and may explain the continual functional improvements (Figure S2). While no attempt was made in this study to maximize miR-206 binding, up to seven binding sites have been placed on other decoy constructs to enhance miR hybridization.[28,29] Further study into the expression profile of miR-206 throughout differentiation and whether it is perturbed in DMD would also aid in the design and timing of our treatment. Co-administration with the AAV-mini-dystrophin generated in our laboratory is another possibility, which could address the primary membrane instability in addition to secondary disease mechanisms and prevent vector loss with muscle degeneration.

In summary, we have identified a pathological role for miR-206 in dystrophic muscle, which promotes secondary pathological mechanisms that exacerbate DMD symptoms. We also show that decreasing miR-206 through AAV9-anti-miR-206 improves motor function and alleviates dystrophic pathology, uncovering a novel therapeutic paradigm for DMD.

MATERIALS AND METHODS

Plasmid Construction and AAV Vector Production

To competitively inhibit miR-206, four tandem repeats of the exact antisense sequence (5′-CCACACACUUCCUUACAUUCCA-3′) were cloned into the pEmbl double-stranded AAV backbone vector containing a cytomegalovirus (CMV) promoter and either a functional (full-length) or non-functional (truncated) GFP reporter gene, which were used for *in vitro* and *in vivo* studies, respectively (Figure 1). The completed constructs were termed "anti-miR-206." The anti-miR-206 constructs and truncated GFP control vector plasmid (without the miR-206 target sequence) were packaged into the AAV2 or AAV9 capsid using the conventional triple transfection method.[43] AAVs were purified by polyethylene glycol (PEG) precipitation followed by two rounds of cesium chloride density gradient ultracentrifugation. Viral titer was quantified by dot blot using the North2South Chemiluminescent Hybridization and Detection Kit (Thermo Fisher Scientific). Densitometric analysis was performed using a standard created with vector plasmid DNA and a biotin-labeled CMV probe (North2South Complete Biotin Random Prime Labeling and Detection Kit, Thermo Fisher Scientific). Vectors were in the range of 2×10^{12} to 1×10^{13} vg/mL.

miR-206 *In Vitro* Specificity Assay

CMV-pre-miR-206 and CMV-pre-miR-124 sequences were packaged into the AAV2 capsid by the triple transfection method. HEK293 cells were transduced with AAV2-anti-miR-206 (containing the full-length GFP) alone or in combination with either AAV2-CMV-pre-miR-206 or AAV2-CMV-pre-miR-124 (MOI, 10^6 vg per cell). GFP expression was observed 48 hr later with a Nikon Eclipse TE300 microscope (Nikon USA, Melville, NY) and imaged with a SPOT RT Slider camera (Diagnostic Instruments, Sterling Heights, MI).

Mice and Vector Administration

Two *mdx* breeding pairs were purchased from the Jackson Laboratory (Bar Harbor, ME) at 6 to 8 weeks old. All animal protocols were approved by the University of North Carolina Animal Care and Use Committee. Eight-week-old male *mdx* mice were randomly assigned to one of four groups: (1) control PBS treated, (2) control sham vector treated, or (3) AAV9-anti-miR-206 treated. AAV9-anti-miR-206 vector was administered via tail vein injection at a dose of 1×10^{12} vg per mouse. Control *mdx* mice were treated with an equal dose of AAV9 vector carrying a truncated GFP ("1/2gfp") or 200 μL PBS solution via tail vein injection. Age-matched WT C57BL/6, untreated, and treated *mdx* mice were sacrificed at 1, 3, or 5 months post-treatment. Animals were anesthetized with an intraperitoneal injection of 2.5% Avertin (tribromoethanol) at a dose of 250 mg/kg. Blood was collected from the jugular vein for serum creatine kinase analysis. Heart, diaphragm (DIA), QUAD, HAM, GAS, and TA muscles were removed bilaterally and weighed. Tissue samples were snap-frozen in liquid nitrogen-cooled isopentane and stored at −80°C for histological and biochemical analysis.

Functional Testing

Functional testing was conducted at 8 weeks old prior to treatment to obtain baseline measurements. Mice were then tested at 1 month post-treatment and every 2 weeks after until sacrifice. Between each test, mice were given 3 to 4 days of rest. A rotarod apparatus (Med Associates, St. Albans, VT) was used to assess motor coordination, balance, and grip. Prior to testing, mice were allowed to acclimate to the stationary rod for 60 s. The rod was then set to accelerate gradually from 4 to 40 rpm over a period of 5 min. After 30 s of running, the time to first fall was recorded to rule out accidental falls from acclimation. Mice that fell within 30 s of the start time were placed back on the rod for a second attempt. The time to fall was used for statistical analysis. A Chatillon DFIS-2 digital grip force meter (Ametek, Largo, FL) was used to test forelimb strength. Forelimb measurements were performed with the meter in tension peak mode. The mouse was allowed to grasp the bar with its front paws in a horizontal position and quickly pulled away from the bar by the tail to obtain a force reading (in grams). Force was measured at least two more times, and bodyweight was recorded at this time for further analysis. Endurance and whole-body function was measured by treadmill running (Harvard Apparatus, Holliston, MA). Mice were placed in a flat treadmill and allowed to acclimate at a speed of 5 m/min for 60 s. The speed was then increased to 10 m/min for a period of 15 min and then increased by 5 m/min every 10 min.

The shock grids at the end of the lanes were set to 1 mA to encourage the mice to run until exhaustion. If a mouse failed to run and remained on the grid for 10 s, the test was terminated and the mouse was removed immediately. The total run time at each speed increment was recorded to calculate total distance for statistical analysis.

Real-Time qPCR

Total RNA was extracted from diaphragm muscle samples using TRIzol reagent (Thermo Fisher Scientific, Carlsbad, CA). RNA yield and quality were determined using a spectrophotometer (model DU640, Beckman Coulter, Brea, CA). To synthesize miRNA-specific cDNA, the miRNA 1st Strand cDNA Synthesis kit (Agilent) was used, starting with 400 ng total RNA. The High-Capacity cDNA Reverse Transcription kit (Thermo Fisher Scientific) was used according to the manufacturer's instructions to create cDNA for mRNA quantitation. The final reaction volumes were diluted 5-fold prior to storage and future analysis. PCR amplification was prepared in triplicate using the PowerUp SYBR Green Master Mix (Thermo Fisher Scientific) as a fluorescence marker and performed in the ABI 7300 real-time PCR system (Thermo Fisher Scientific). For miRNA quantitation, miR-26b was used as an endogenous control. Beta-actin was used as an endogenous control for mRNA quantitation. Primer sequences are described in Table S1. Relative expression levels were calculated by the cycle threshold method.

Western Blot Analysis

For VEGF-A detection, TA muscle samples were homogenized in radioimmunoprecipitation assay (RIPA) lysis buffer (150 mM NaCl, 1% Triton X-100, 0.5% sodium deoxycholate, 0.1% SDS, 50 mM Tris [pH 7.5], 1 mM PMSF and protease inhibitor cocktail [Sigma-Aldrich, St. Louis, MO]). Protein samples (20 μg) were denatured in reducing buffer (62.5 mM Tris-HCl [pH 6.8], 1.5% SDS, 8.3% glycerol, 1.5% beta-mercaptoethanol, 0.005% bromophenol blue) and separated by electrophoresis on 12% SDS-polyacrylamide gels with prestained standards (Fermentas PageRuler Plus Prestained Protein Ladder, Thermo Fisher Scientific). After separation, proteins were transferred onto a polyvinylidene fluoride (PVDF) membrane (0.2 μm) with transfer buffer (25 mM Tris, 190 mM glycine, 20% methanol) at 225 mA for 1.5 hr. GAS samples were homogenized in dystrophin lysis buffer (4% SDS, 125 mM Tris [pH 8.8], 4% glycerol, 1 mM PMSF and protease inhibitor cocktail [Sigma-Aldrich]) for utrophin detection. Protein samples (50 μg for utrophin detection and 20 μg for loading control) were denatured in dystrophin loading buffer (4% SDS, 125 mM Tris [pH 8.8], 4% glycerol, 100 mM dithiothreitol, 0.01% bromophenol blue) and separated by electrophoresis on SDS-polyacrylamide gels (6.5% for utrophin detection and 12% for loading control) with pre-stained standards. Separated proteins were transferred onto a PVDF membrane (0.45 μm) using transfer buffer for large molecular weight proteins (25 mM Tris, 190 mM glycine, 20% methanol, 0.1% SDS) at 270 mA for 2 hr on ice. Immunoblots were blocked with 5% non-fat dry milk in Tris-buffered saline (TBS)-0.1% Tween for 1 hr at room temperature then washed three times in 0.1% TBS-Tween (TBS-T) for 10 min each. Blots were incubated with a rabbit polyclonal antibody against human VEGFA (1:1,000, ab46154, Abcam, Cambridge, MA), a goat polyclonal antibody against human utrophin (1:1,000, sc-7459, Santa Cruz Biotechnology, Dallas, TX) or a rabbit polyclonal antibody against mouse glyceraldehyde 3-phosphate dehydrogenase (GAPDH; 1:10,000, G9545, Sigma-Aldrich) in 3% BSA in 0.1% TBS-T overnight at 4°C. Membranes were washed three times in 0.1% TBS-T for 10 min each, then incubated with peroxidase-conjugated goat anti-rabbit (1:5,000, A0545, Sigma-Aldrich) or rabbit anti-goat immunoglobulin G (IgG) (1:5,000, A5420, Sigma-Aldrich) in 3% BSA for 1 hr at room temperature. After washing, the membranes were developed with Western Lightening ECL Pro reagent (PerkinElmer, Waltham, MA) according to the manufacturer's protocol. Images were acquired using the FluorChem M system (ProteinSimple) and analyzed using Alphaview 3.3.1.0 software (ProteinSimple). Band intensity was normalized to GAPDH expression for densitometric analysis.

Histological Staining

Transverse cryostat sections 10 um thick were made from heart, DIA, QUAD, HAM, GAS, and TA muscle. H&E staining was performed according to standard protocol. Masson trichrome staining was performed on DIA muscle according to manufacturer's instructions (IMEB, San Marcos, CA). DIA and HAM sections were stained with Fast green and Picrosirius red according to standard protocol to observe collagen deposition. Slides were examined with a Nikon Eclipse TE300 microscope (Nikon USA, Melville, NY) and imaged with a SPOT RT Slider camera (Diagnostic Instruments, Sterling Heights, MI). Images were analyzed using ImageJ software. Picrosirius red was quantified using the *Threshold_Color* plugin and expressed as a percentage of total area.

Immunohistochemistry

Capillary-to-muscle fiber ratios were determined by immunostaining DIA sections. Sections were blocked with 10% horse serum. Muscle fibers were stained using a rat monoclonal antibody against laminin alpha-2 (1:500, L0663, Sigma-Aldrich) and vessels stained with a rhodamine-conjugated *Griffonia simplifica I* lectin (1:100, #RL-1102, Vector Laboratories, Burlingame, CA). Slides were washed three times in 0.1% PBS-Tween. An Alexa Fluor 488-conjugated chicken anti-rat IgG (1:800, #A21470, Molecular Probes, Eugene, OR) was used to visualize laminin staining. To examine utrophin localization, sections were first blocked in 10% horse serum and then incubated with a goat anti-utrophin polyclonal antibody (1:100, #sc-7459, Santa Cruz Biotechnology) overnight at 4°C. Sections were then incubated with a Cy3-conjugated anti-goat IgG (1:500, Jackson ImmunoResearch Laboratories, West Grove, PA). Unless otherwise specified, incubations were at room temperature for 1 hr. Slides were examined with a Zeiss Axiovert 200M microscope (Carl Zeiss USA, Peabody, MA). Images were acquired with an AxioCam MRm (Zeiss), processed with AxioVision Rel 4.6 software (Zeiss) and analyzed using ImageJ software.

Modified Miles Assay

To compare vessel permeability, a modified Miles assay was performed as described in Radu and Chernoff[44] EB dye (0.01% solution,

final dose of 2 mg per mouse, Sigma-Aldrich) was administered to WT, untreated, and treated *mdx* mice at 3 and 5 months post-treatment via tail-vein injection. After 30 min, the mice were anesthetized with Avertin as mentioned above (Mice and Vector Administration). After cervical dislocation, DIA, QUAD, HAM, GAS and TA muscles were removed. Muscles were weighed and placed in 500 μL formamide (Thermo Fisher Scientific). To extract dye, samples were incubated at 37°C for 24 hr. The absorbance of the resultant solution for each sample and an EB standard were measured at 595 nm in a Wallac Victor^2 1420 Multilabel Counter plate reader (PerkinElmer, Waltham, MA). Results were expressed as ng of dye per mg muscle.

Hydroxyproline Assay

To measure fibrosis, DIA tissue samples from WT, untreated, and treated *mdx* were dried under vacuum and weighed. Hydroxyproline content was measured according to a previously described method.[45] Collagen content was ascribed to the amount of hydroxyproline (~13.5% of total collagen) in each sample.

Statistical Analysis

Values are expressed as mean ± SEM. Welch's t test was applied when comparing two groups. When comparing three groups, one-way ANOVA was applied using GraphPad Prism 5.0 software (GraphPad Software, La Jolla, CA). A p value < 0.05 was considered statistically significant.

SUPPLEMENTAL INFORMATION

Supplemental Information includes Supplemental Materials and Methods, five figures, and one table and can be found with this article online at https://doi.org/10.1016/j.omtn.2018.05.011.

AUTHOR CONTRIBUTIONS

Conceptualization, K.B., B.X., X.X.; Methodology, K.B., B.X., X.X.; Validation, K.B., C.Q., Jianbin L., T.P., Juan L; Formal Analysis, K.B.; Investigation, K.B., B.X.; Resources, K.B., Jianbin L., Juan L.; Writing – Original Draft, K.B.; Writing – Review & Editing, K.B., C.Q., Q.J., X.X.; Visualization, K.B.; Supervision, B.X., C.Q., Juan L., X.X.; Project Administration, Jianbin L., Juan L.; Funding Acquisition, K.B., X.X.

ACKNOWLEDGMENTS

Research reported in this publication was supported by the National Institute of Arthritis and Musculoskeletal and Skin Diseases under award number 1F31AR068877 and the National Institute of Neurological Disorders and Stroke under award number 5R01NS079568. The content is solely the responsibility of the authors and does not necessarily represent the official views of the NIH.

REFERENCES

1. Sussman, M. (2002). Duchenne muscular dystrophy. J. Am. Acad. Orthop. Surg. *10*, 138–151.

2. Qiao, C., Koo, T., Li, J., Xiao, X., and Dickson, J.G. (2011). Gene therapy in skeletal muscle mediated by adeno-associated virus vectors. Methods Mol. Biol. *807*, 119–140.

3. Wang, B., Li, J., and Xiao, X. (2000). Adeno-associated virus vector carrying human minidystrophin genes effectively ameliorates muscular dystrophy in mdx mouse model. Proc. Natl. Acad. Sci. USA *97*, 13714–13719.

4. Watchko, J., O'Day, T., Wang, B., Zhou, L., Tang, Y., Li, J., and Xiao, X. (2002). Adeno-associated virus vector-mediated minidystrophin gene therapy improves dystrophic muscle contractile function in mdx mice. Hum. Gene Ther. *13*, 1451–1460.

5. Yokota, T., Lu, Q.L., Partridge, T., Kobayashi, M., Nakamura, A., Takeda, S., and Hoffman, E. (2009). Efficacy of systemic morpholino exon-skipping in Duchenne dystrophy dogs. Ann. Neurol. *65*, 667–676.

6. Cirak, S., Arechavala-Gomeza, V., Guglieri, M., Feng, L., Torelli, S., Anthony, K., Abbs, S., Garralda, M.E., Bourke, J., Wells, D.J., et al. (2011). Exon skipping and dystrophin restoration in patients with Duchenne muscular dystrophy after systemic phosphorodiamidate morpholino oligomer treatment: an open-label, phase 2, dose-escalation study. Lancet *378*, 595–605.

7. Sakamoto, M., Yuasa, K., Yoshimura, M., Yokota, T., Ikemoto, T., Suzuki, M., Dickson, G., Miyagoe-Suzuki, Y., and Takeda, S. (2002). Micro-dystrophin cDNA ameliorates dystrophic phenotypes when introduced into mdx mice as a transgene. Biochem. Biophys. Res. Commun. *293*, 1265–1272.

8. Kornegay, J.N., Li, J., Bogan, J.R., Bogan, D.J., Chen, C., Zheng, H., Wang, B., Qiao, C., Howard, J.F., Jr., and Xiao, X. (2010). Widespread muscle expression of an AAV9 human mini-dystrophin vector after intravenous injection in neonatal dystrophin-deficient dogs. Mol. Ther. *18*, 1501–1508.

9. Mendell, J.R., Campbell, K., Rodino-Klapac, L., Sahenk, Z., Shilling, C., Lewis, S., Bowles, D., Gray, S., Li, C., Galloway, G., et al. (2010). Dystrophin immunity in Duchenne's muscular dystrophy. N. Engl. J. Med. *363*, 1429–1437.

10. Thomas, G.D. (2013). Functional muscle ischemia in Duchenne and Becker muscular dystrophy. Front. Physiol. *4*, 381.

11. Rosenberg, A.S., Puig, M., Nagaraju, K., Hoffman, E.P., Villalta, S.A., Rao, V.A., Wakefield, L.M., and Woodcock, J. (2015). Immune-mediated pathology in Duchenne muscular dystrophy. Sci. Transl. Med. *7*, 299rv4.

12. Deconinck, N., and Dan, B. (2007). Pathophysiology of duchenne muscular dystrophy: current hypotheses. Pediatr. Neurol. *36*, 1–7.

13. Asai, A., Sahani, N., Kaneki, M., Ouchi, Y., Martyn, J.A., and Yasuhara, S.E. (2007). Primary role of functional ischemia, quantitative evidence for the two-hit mechanism, and phosphodiesterase-5 inhibitor therapy in mouse muscular dystrophy. PLoS ONE *2*, e806.

14. Ennen, J.P., Verma, M., and Asakura, A. (2013). Vascular-targeted therapies for Duchenne muscular dystrophy. Skelet. Muscle *3*, 9.

15. Engvall, E., and Wewer, U.M. (2003). The new frontier in muscular dystrophy research: booster genes. FASEB J. *17*, 1579–1584.

16. Messina, S., Mazzeo, A., Bitto, A., Aguennouz, M., Migliorato, A., De Pasquale, M.G., Minutoli, L., Altavilla, D., Zentilin, L., Giacca, M., et al. (2007). VEGF overexpression via adeno-associated virus gene transfer promotes skeletal muscle regeneration and enhances muscle function in mdx mice. FASEB J. *21*, 3737–3746.

17. Tinsley, J.M., Fairclough, R.J., Storer, R., Wilkes, F.J., Potter, A.C., Squire, S.E., Powell, D.S., Cozzoli, A., Capogrosso, R.F., Lambert, A., et al. (2011). Daily treatment with SMTC1100, a novel small molecule utrophin upregulator, dramatically reduces the dystrophic symptoms in the mdx mouse. PLoS ONE *6*, e19189.

18. Tinsley, J., Deconinck, N., Fisher, R., Kahn, D., Phelps, S., Gillis, J.M., and Davies, K. (1998). Expression of full-length utrophin prevents muscular dystrophy in mdx mice. Nat. Med. *4*, 1441–1444.

19. Deconinck, N., Tinsley, J., De Backer, F., Fisher, R., Kahn, D., Phelps, S., Davies, K., and Gillis, J.M. (1997). Expression of truncated utrophin leads to major functional improvements in dystrophin-deficient muscles of mice. Nat. Med. *3*, 1216–1221.

20. Tinsley, J., Robinson, N., Wilson, F., Horne, G., and Davies, K. (2014). Future clinical and biomarker development for SMT C1100, the first utrophin modulator to enter clinical trials for Duchenne muscular dystrophy (DMD) (S6.004). Neurology *82* (*Suppl 10*), S6.004.

21. Odom, G.L., Gregorevic, P., Allen, J.M., Finn, E., and Chamberlain, J.S. (2008). Microutrophin delivery through rAAV6 increases lifespan and improves muscle

function in dystrophic dystrophin/utrophin-deficient mice. Mol. Ther. *16*, 1539–1545.

22. Bartel, D.P. (2009). MicroRNAs: target recognition and regulatory functions. Cell *136*, 215–233.
23. Greco, S., De Simone, M., Colussi, C., Zaccagnini, G., Fasanaro, P., Pescatori, M., Cardani, R., Perbellini, R., Isaia, E., Sale, P., et al. (2009). Common micro-RNA signature in skeletal muscle damage and regeneration induced by Duchenne muscular dystrophy and acute ischemia. FASEB J. *23*, 3335–3346.
24. McCarthy, J.J., Esser, K.A., and Andrade, F.H. (2007). MicroRNA-206 is overexpressed in the diaphragm but not the hindlimb muscle of mdx mouse. Am. J. Physiol. Cell Physiol. *293*, C451–C457.
25. Chen, J.-F., Tao, Y., Li, J., Deng, Z., Yan, Z., Xiao, X., and Wang, D.Z. (2010). microRNA-1 and microRNA-206 regulate skeletal muscle satellite cell proliferation and differentiation by repressing Pax7. J. Cell Biol. *190*, 867–879.
26. Lin, C.-Y., Lee, H.C., Fu, C.Y., Ding, Y.Y., Chen, J.S., Lee, M.H., Huang, W.J., and Tsai, H.J. (2013). MiR-1 and miR-206 target different genes to have opposing roles during angiogenesis in zebrafish embryos. Nat. Commun. *4*, 2829.
27. Rosenberg, M.I., Georges, S.A., Asawachaicharn, A., Analau, E., and Tapscott, S.J. (2006). MyoD inhibits Fstl1 and Utrn expression by inducing transcription of miR-206. J. Cell Biol. *175*, 77–85.
28. Ebert, M.S., Neilson, J.R., and Sharp, P.A. (2007). MicroRNA sponges: competitive inhibitors of small RNAs in mammalian cells. Nat. Methods *4*, 721–726.
29. Ebert, M.S., and Sharp, P.A. (2010). MicroRNA sponges: progress and possibilities. RNA *16*, 2043–2050.
30. Kutay, H., Bai, S., Datta, J., Motiwala, T., Pogribny, I., Frankel, W., Jacob, S.T., and Ghoshal, K. (2006). Downregulation of miR-122 in the rodent and human hepatocellular carcinomas. J. Cell. Biochem. *99*, 671–678.
31. Banzhaf-Strathmann, J., Benito, E., May, S., Arzberger, T., Tahirovic, S., Kretzschmar, H., Fischer, A., and Edbauer, D. (2014). MicroRNA-125b induces tau hyperphosphorylation and cognitive deficits in Alzheimer's disease. EMBO J. *33*, 1667–1680.
32. Arnett, A.L.H., Konieczny, P., Ramos, J.N., Hall, J., Odom, G., Yablonka-Reuveni, Z., Chamberlain, J.R., and Chamberlain, J.S. (2014). Adeno-associated viral (AAV) vectors do not efficiently target muscle satellite cells. Mol. Ther. Methods Clin. Dev. , Published online September 17, 2014. https://doi.org/10.1038/mtm2014.38.
33. Liu, N., Williams, A.H., Maxeiner, J.M., Bezprozvannaya, S., Shelton, J.M., Richardson, J.A., Bassel-Duby, R., and Olson, E.N. (2012). microRNA-206 promotes skeletal muscle regeneration and delays progression of Duchenne muscular dystrophy in mice. J. Clin. Invest. *122*, 2054–2065.
34. Anderson, J.E., Garrett, K., Moor, A., McIntosh, L., and Penner, K. (1998). Dystrophy and myogenesis in mdx diaphragm muscle. Muscle Nerve *21*, 1153–1165.
35. Willmann, R., Possekel, S., Dubach-Powell, J., Meier, T., and Ruegg, M.A. (2009). Mammalian animal models for Duchenne muscular dystrophy. Neuromuscul. Disord. *19*, 241–249.
36. Aartsma-Rus, A., and van Putten, M. (2014). Assessing functional performance in the Mdx mouse model. J. Vis. Exp. *2014*, e51303.
37. Carmeliet, P. (2000). VEGF gene therapy: stimulating angiogenesis or angioma-genesis? Nat. Med. *6*, 1102–1103.
38. Nelson, M.D., Rader, F., Tang, X., Tavyev, J., Nelson, S.F., Miceli, M.C., Elashoff, R.M., Sweeney, H.L., and Victor, R.G. (2014). PDE5 inhibition alleviates functional muscle ischemia in boys with Duchenne muscular dystrophy. Neurology *82*, 2085–2091.
39. Adamo, C.M., Dai, D.F., Percival, J.M., Minami, E., Willis, M.S., Patrucco, E., Froehner, S.C., and Beavo, J.A. (2010). Sildenafil reverses cardiac dysfunction in the mdx mouse model of Duchenne muscular dystrophy. Proc. Natl. Acad. Sci. USA *107*, 19079–19083.
40. Verma, M., Asakura, Y., Hirai, H., Watanabe, S., Tastad, C., Fong, G.H., Ema, M., Call, J.A., Lowe, D.A., and Asakura, A. (2010). Flt-1 haploinsufficiency ameliorates muscular dystrophy phenotype by developmentally increased vasculature in mdx mice. Hum. Mol. Genet. *19*, 4145–4159.
41. Khurana, T.S., and Davies, K.E. (2003). Pharmacological strategies for muscular dystrophy. Nat. Rev. Drug Discov. *2*, 379–390.
42. Handschin, C., Kobayashi, Y.M., Chin, S., Seale, P., Campbell, K.P., and Spiegelman, B.M. (2007). PGC-1α regulates the neuromuscular junction program and ameliorates Duchenne muscular dystrophy. Genes Dev. *21*, 770–783.
43. Xiao, X., Li, J., and Samulski, R.J. (1998). Production of high-titer recombinant adeno-associated virus vectors in the absence of helper adenovirus. J. Virol. *72*, 2224–2232.
44. Radu, M., and Chernoff, J. (2013). An in vivo assay to test blood vessel permeability. J. Vis. Exp. *2014*, e50062.
45. Carlson, C. (2009). Determination of hydroxyproline content as a measure of fibrosis in nondystrophic and dystrophic skeletal muscle. http://www.treat-nmd.eu/downloads/file/sops/dmd/MDX/DMD_M.1.2.006.pdf.